The Influence of the Vibration Suppression on the Rotor Crack Detection Performance

L. S. Leão[1], A. Sahinkaya[2], A. A. Cavalini Jr.[1(✉)], V. Steffen Jr.[1], and J. T. Sawicki[2]

[1] LMEst – Structural Mechanics Laboratory, School of Mechanical Engineering, Federal University of Uberlândia, Av. João Naves de Ávila, 2121, Uberlândia, MG 38408-196, Brazil
aacjunior@ufu.br

[2] RoMaDyC – Center for Rotating Machinery Dynamics and Control, Washkewicz College of Engineering, Cleveland State University, 1960 East 24th Street, FH 262, Cleveland, OH 44115, USA

Abstract. The feasibility of controlling the vibrations of rotating machines while performing online crack detection is addressed in this paper. For this purpose, two controllers are compared, namely *LQR* and H_∞, which represent optimal and robust control strategies, respectively. A non-dimensional Jeffcott rotor model is employed to simulate the dynamic behavior of a rotating machine. In addition, a crack is introduced in the shaft using the so-called Mayes' model. An active magnetic bearing (AMB) is placed as an actuator at the disc location along the rotor. For each control technique, different strategies are implemented to evaluate their effectiveness on both attenuating the vibration level and detecting the fatigue crack. Conclusions are drawn regarding the effectiveness of the control strategy for each phenomenon.

Keywords: Active magnetic bearing · Rotordynamics
Structural health monitoring · On-line crack detection · Optimal control
Robust control

1 Introduction

Active Magnetic Bearing (AMB) is a mechatronic device that is able to apply a magnetic field to generate control forces in rotating shafts. This means that the position of the shaft is continuously sensed and the magnetic fields are actively manipulated for maintaining the rotor position, according to desired design specifications. AMBs play the role of supporting the shaft by levitation, which presents several advantages as compared with traditional mechanical or fluid-film bearings, such as no mechanic contact, lubrication free, no wear, low friction, etc. Moreover, they can be placed along the rotor shaft to apply radial and/or axial forces that can meet different objectives, which are related to both vibration control and health monitoring. A number of AMBs applications on rotordynamics have been published during the last years; however, the majority of the contributions are focused on vibration control [1–4].

K. L. Cavalca and H. I. Weber (Eds.): IFToMM 2018, MMS 63, pp. 175–189, 2019.
https://doi.org/10.1007/978-3-319-99272-3_13

In this paper, the AMBs' capacity of performing online structural health monitoring (SHM), combined with vibration control, will be explored. Online SHM techniques have become more interesting for the industry since inspections can be performed while the rotating machinery is under operation condition. Besides, scheduled shut-downs can be considerably reduced [5]. Classical online diagnostics techniques are based on vibration signature analyses, which require very simple and commercially available instrumentation.

Several papers can be found in the literature dealing with the use of AMBs in the context of SHM. The techniques conveyed, such as combination resonances [6], multifractal analysis [7], recurrence plots [8], multiresolution wavelet analysis [9], auxiliary state variables [10], linear matrix inequalities [11], among others, have been tested both numerical and experimentally.

According to Zhu et al. [12], the use of AMBs for attenuating rotor vibrations impairs SHM techniques, since the AMBs serve as a filter, being able to suppress harmonics all over the frequency range. Therefore, in the present paper, AMBs are dedicated to rotor vibration control; however, the control law can be modified as necessary, so that the super-harmonics become detectable on the rotor spectrum response. For this purpose, a model of Jeffcott rotor is used, having a crack modeled by using the so-called Mayes' model. Two different controllers will be compared, namely the *LQR* and H_∞, and conclusions will derive from the results obtained.

2 Jeffcott Rotor Model

A Jeffcott rotor model is analysed in this paper. A massless elastic shaft containing a rigid disc located at the shaft mid-span and supported by simple rigid bearings characterizes this model (Fig. 1).

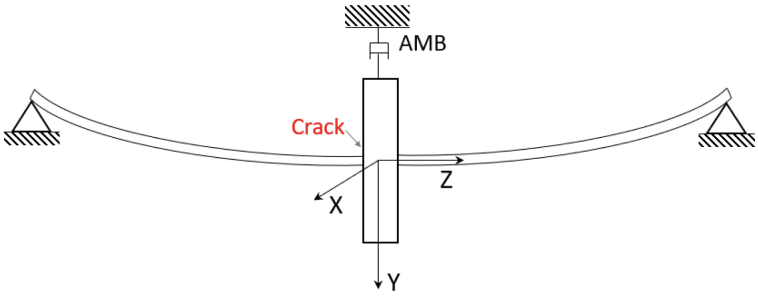

Fig. 1. Jeffcott rotor with transverse crack and AMB actuator.

An AMB is placed at the disc position, so that control forces acting on the rotor will appear according to a given control law. Finally, a crack is located close to the disc and its model will be explained in the following section.

Two coordinate frames are necessary to write the equations of motion of the rotor system, as follows: OXY fixed in space and $O\eta\xi$,which rotates with the same angular speed of the shaft, where ξ is assumed to be perpendicular to the crack edge. Figure 2 presents both reference frames for a cracked shaft subjected to an unbalance me_μ, where m stands for the unbalance mass, e_μ indicates its unbalance eccentricity, and β represents its angular distance from the rotating ξ axis. The hatched area indicates the cracked part of the shaft and ω_{op} represents the operational speed.

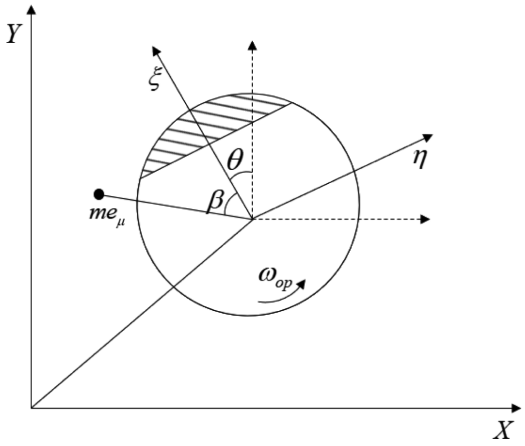

Fig. 2. Two coordinate frames on the cracked rotor: an inertial and a rotating reference system.

The equations of motion for a Jeffcott rotor subjected to a breathing crack in the presence of the AMB forces are derived from Newton's second law, considering the inertial coordinate system. These equations are written in the matrix form, Eq. (1), with the motion occurring along the X and Y directions:

$$\begin{bmatrix} m & 0 \\ 0 & m \end{bmatrix} \begin{Bmatrix} \ddot{x} \\ \ddot{y} \end{Bmatrix} + \begin{bmatrix} c & 0 \\ 0 & c \end{bmatrix} \begin{Bmatrix} \dot{x} \\ \dot{y} \end{Bmatrix} + \boldsymbol{K}(t) \begin{Bmatrix} x \\ y \end{Bmatrix} = \begin{Bmatrix} 0 \\ mg \end{Bmatrix} + me_\mu \omega^2 \begin{Bmatrix} \cos(\omega t + \beta) \\ \sin(\omega t + \beta) \end{Bmatrix} + \begin{Bmatrix} F_x \\ F_y \end{Bmatrix} \tag{1}$$

On the left-hand side of Eq. (1) it can be observed that the matrices of mass and damping are uncoupled. The gyroscopic effect is not taken into account due to the assumptions made for the Jeffcott rotor model. On the other hand, the stiffness matrix is a function of time due to the breathing behavior of the crack. On the right-hand side of Eq. (1), one can see the weight of the rotor, the unbalance efforts, and the external AMB control force, respectively.

In Sect. 6, one explains how the components of the AMB control force will be affected by the control strategies chosen, for both *LQR* and H_∞ synthesis.

3 Crack Model

Two of the most widely used methods for modeling the breathing behavior of transversal cracks are the so-called Gasch's [13, 14] and Mayes' [15, 16] models. These methods are considered valid when the weight dominance assumption is respected, in which static loads are higher than the dynamic ones. It represents a simplification because it converts the nonlinear equation of motion to a linear equation with time-varying coefficients [17]. It is worth mentioning that a more sophisticated crack model could be used at this point, namely the flex model (as based on the stress distribution on the crack), as proposed in [24].

The approach proposed by Mayes is chosen in this work since it represents the breathing behavior of the crack more realistically. In this model, the crack opening and closure are weighted by a cosine function, according to Eq. (2).

$$\begin{aligned} k_{\xi Mayes}(\theta) &= \frac{1}{2}(k_o + k_\xi) + \frac{1}{2}(k_o - k_\xi)C_1 \\ k_{\eta Mayes}(\theta) &= \frac{1}{2}(k_o + k_\eta) + \frac{1}{2}(k_o - k_\eta)C_1 \end{aligned} \tag{2}$$

where $C_1 = \cos(\theta)$ ($C_i = \cos(i\theta)$, $i = 1, 2, 3, \ldots$); k_o is the stiffness of the shaft without crack; k_η and k_ξ are the stiffness of the shaft with a crack along the directions η and ξ, respectively. According to Fig. 2, if $C_1 = 1$, i.e., for $\theta = 0^0$, $k_{\xi Mayes}(0^0) = k_o$ and $k_{\eta Mayes}(0^0) = k_o$, because the crack is fully closed. However, if $C_1 = -1$, i.e., for $\theta = 180^0$ $k_{\xi Mayes}(180^0) = k_\xi$ and $k_{\eta Mayes}(180^0) = k_\eta$, which are the reduced stiffness, for the fully opened crack [18].

The stiffness of the cracked shaft, in rotating coordinates ($\boldsymbol{K}_{RMayes}$ in the matrix representation, according to the Mayes' model) is given by:

$$\boldsymbol{K}_{RMayes} = \begin{bmatrix} k_{M\xi} + k_{D\xi}C_1 & 0 \\ 0 & k_{M\eta} + k_{D\eta}C_1 \end{bmatrix} \tag{3}$$

Where $k_{M\xi} = (k_o + k_\xi)/2$, $k_{D\xi} = (k_o - k_\xi)/2$, $k_{M\eta} = (k_o + k_\eta)/2$ and $k_{D\eta} = (k_o - k_\eta)/2$.

On the other hand, the stiffness of the cracked shaft in fixed coordinates, $\boldsymbol{K}_{FMayes}$, is determined from the mathematical transformation shown in Eq. (4).

$$\boldsymbol{K}_{FMayes} = \begin{bmatrix} C_1 & S_1 \\ -S_1 & C_1 \end{bmatrix}^T \boldsymbol{K}_{RMayes} \begin{bmatrix} C_1 & S_1 \\ -S_1 & C_1 \end{bmatrix} = \begin{bmatrix} k_{FMayes\,(11)} & k_{FMayes\,(12)} \\ k_{FMayes\,(12)} & k_{FMayes\,(22)} \end{bmatrix} \tag{4}$$

where $S_i = \sin(i\theta)$, $i = 1, 2, 3, \ldots$.

In this contribution, the stiffness matrix $\boldsymbol{K}_{FMayes}$ is used in the matrix equation of motion of the cracked shaft, by replacing adequately the term $\boldsymbol{K}(t)$ in Eq. (1).

4 AMB Model

The AMB actuator is responsible for applying magnetic forces to the shaft, which are proportional to the air gap and to the electrical currents applied to the coils.

In this contribution, a radial AMB actuator composed of two pairs of horseshoe coils, symmetrically mounted and coincident with the X and Y directions is considered, as shown in Fig. 3.

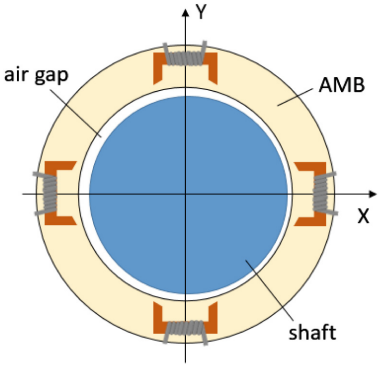

Fig. 3. Active Magnetic Bearing (AMB); adapted from [19]

The most common AMB applications are dedicated to the attenuation of the vibrations associated with the dynamic responses of rotating machines. Due to its efficiency, the control action makes the crack identification procedure quite difficult, since the peaks of the response signature are damped out. Two control techniques will be tested in the present paper: (i) based only on vibration suppression, and (ii) based on crack detection, by keeping the 2X and/or 3X vibration harmonics in the spectrum.

After linearization (using a Taylor expansion around a chosen position), one can present the AMB forces according to Eq. (5).

$$\begin{Bmatrix} F_x \\ F_y \end{Bmatrix} = \begin{bmatrix} k_{Xx} & 0 \\ 0 & k_{Xy} \end{bmatrix} \begin{Bmatrix} x \\ y \end{Bmatrix} + \begin{bmatrix} k_{Ix} & 0 \\ 0 & k_{Iy} \end{bmatrix} \begin{Bmatrix} i_x \\ i_y \end{Bmatrix} = \boldsymbol{K_X x} + \boldsymbol{K_I i_c} \tag{5}$$

where $\boldsymbol{K_X}$ is the so-called displacement stiffness and relates the shaft position to the AMB force along both directions of the vector $\boldsymbol{x}$, and $\boldsymbol{K_I}$ represents the current stiffness, which relates the applied control currents $\boldsymbol{i_c}$ to the AMB forces.

According to [12], the displacement and current stiffness can be defined, respectively, as:

$$\begin{aligned} k_{Xx} &= \mu_0 A N^2 i_{ox}^2 / s^3 \qquad k_{Xy} = \mu_0 A N^2 i_{oy}^2 / s^3 \\ k_{Ix} &= -\mu_0 A N^2 i_{ox} / s^2 \qquad k_{Iy} = -\mu_0 A N^2 i_{oy} / s^2 \end{aligned} \tag{6}$$

where $\mu_0 = 4\pi E - 7H/m$ stands for the air permeability, A represents the cross-sectional flux area of the air-gap, N indicates the number of windings of the coil, i_{ox} and i_{oy} represent the bias currents at directions X and Y, respectively, and s stands for the nominal air-gap.

The AMB forces in both X and Y directions, presented by Eq. (5), are now introduced into Eq. (1) and will be influenced by the control strategies presented in Sect. 6. The following step aims at transforming the rotor equation of motion into a convenient non-dimensional equation.

5 Non-dimensional Equation of Motion of a Cracked Rotor Controlled by an AMB

The general equation of motion for a cracked Jeffcott rotor with an AMB device is obtained by substituting Eqs. (4) and (5) into Eq. (1). Since in the present case the interest is focused on the vibration components at the operation speed (1X, 2X, and 3X), one divides both sides of this expression by $m\omega^2\delta_{st}$, thus leading to Eq. (7).

$$\begin{bmatrix} 1 & 0 \\ 0 & 1 \end{bmatrix} \begin{Bmatrix} X'' \\ Y'' \end{Bmatrix} + \frac{1}{\Omega} \begin{bmatrix} 2\zeta & 0 \\ 0 & 2\zeta \end{bmatrix} \begin{Bmatrix} X' \\ Y' \end{Bmatrix} + \frac{1}{k_0\Omega^2} \begin{bmatrix} k_{FMayes\,(11)} - k_{Xx} & k_{FMayes\,(12)} \\ k_{FMayes\,(12)} & k_{FMayes\,(22)} - k_{Xy} \end{bmatrix} \begin{Bmatrix} X \\ Y \end{Bmatrix} = \frac{1}{\Omega^2} \begin{Bmatrix} 0 \\ 1 \end{Bmatrix} + U \begin{Bmatrix} \cos(\tau + \beta) \\ \sin(\tau + \beta) \end{Bmatrix} + \frac{1}{mg\Omega^2} \begin{bmatrix} k_{Ix} & 0 \\ 0 & k_{Iy} \end{bmatrix} \begin{Bmatrix} i_x \\ i_y \end{Bmatrix} \tag{7}$$

where the prime stands for the differentiation with respect to the non-dimensional time, $\tau = \omega t$, $X = x/\delta_{st}$ and $Y = y/\delta_{st}$, δ_{st} is the static deflection of the shaft at the disc position due to its weight, $\Omega = \omega_{op}/\omega_c$ is the rotational speed ratio (relates the operational and the critical $\omega_c = \sqrt{k_0/m}$ speeds of the rotor), $\zeta = c/2m\omega_c$ is the viscous damping ratio, and $U = e_\mu/\delta_{st}$ is the parameter related to the rotor unbalance.

6 Control Techniques –Brief Review

In this section, the theoretical background regarding the vibration control techniques used in this paper is presented, i.e., *LQR* and H_∞ synthesis. For this purpose, the equation of motion of the system is presented in the state-space form. This is the standard format used to model a control problem and aims at finding a relation between the system states.

It is worth mentioning that the considered control techniques have a direct influence on the AMB forces and, consequently, affecting the lateral vibration amplitudes of the cracked shaft. Thus, this section presents formulation responsible for changing the values of the last term in the right-hand side of Eq. (1) decreasing the lateral vibration amplitudes of the rotating machine.

6.1 *LQR* Controller Synthesis [20]

Consider a system where all the states are known, either by measurement or through an observer, and all the inputs can be considered deterministic, in state-space arrangement:

$$\begin{aligned} \dot{\boldsymbol{x}} &= \boldsymbol{A}\boldsymbol{x} + \boldsymbol{B}\boldsymbol{u} \\ \boldsymbol{y} &= \boldsymbol{C}\boldsymbol{x} \end{aligned} \tag{8}$$

The purpose of the controller is to alter the input to the system so that the controlled system will present a desired dynamic behavior. The Linear Quadratic Regulator (*LQR*) represents an optimal full state feedback controller. This technique requires the system to be linear, time invariant (LTI), and deterministic. Therefore, in the case of the present paper, the control gain will be derived by considering a healthy rotor system, i.e., in Eq. (7) the stiffness matrix will be $\boldsymbol{K}_{healthy} = diag(K_0)$.

The optimal control is based on optimization processes, which involve the minimization of a cost function. In the case of a continuous-time LQR control, the cost function is given by Eq. (9):

$$\boldsymbol{J}_r = \int_0^\infty \left(\boldsymbol{x}(t)^T \boldsymbol{Q}\boldsymbol{x}(t) + \boldsymbol{u}(t)^T \boldsymbol{R}\boldsymbol{u}(t)\right) dt \tag{9}$$

where $\boldsymbol{Q}$ and $\boldsymbol{R}$ are positive semi-definite symmetric matrices.

The purpose of the cost function is to minimize the control effort and energy of the states. The $\boldsymbol{Q}$ and $\boldsymbol{R}$ matrices are used to determine the importance of each objective. A low ratio between matrices $\boldsymbol{Q}$ and $\boldsymbol{R}$ implies weak control, whereas a high ratio implies more performant control. The solution of the optimization problem can be written as a static gain $\boldsymbol{K}_r$, which leads to the following control law:

$$\boldsymbol{u}(t) = \boldsymbol{K}_r \boldsymbol{x}(t) \tag{10}$$

For defining the new rotor system controlled by the *LQR* technique, the control law expressed by Eq. (10) is substituted into Eq. (8), which changes the dynamics of the system as written by Eq. (11).

$$\dot{\boldsymbol{x}} = \boldsymbol{A}_K \boldsymbol{x} \tag{11}$$

where $\boldsymbol{A}_K = (\boldsymbol{A} - \boldsymbol{B}\boldsymbol{K}_r)$ represents the close loop state dynamics matrix.

6.2 H_∞ Synthesis [21]

Similar to *LQR*, the H_∞ control technique is model-based and formulated by considering the healthy rotor system. However, H_∞ synthesis stands for a more sophisticated controller, representing an additional dynamic system instead of simple static gains.

It is well known that the goal of the H_∞ synthesis is to find a stabilizing control matrix $\boldsymbol{K}$, such that the gain of the closed-loop plant is smaller than a certain target Υ [20, 21]. In this paper, the target is defined as the unitary value, according to Eq. (12).

$$\|F_l(\boldsymbol{G},\boldsymbol{K})\|_\infty < \gamma \text{ and } \gamma = 1 \tag{12}$$

The idea behind setting Υ to 1 is to make sure that the desired performance is achieved in the presence of expected disturbances. This can be easily seen from the definition of H_∞ norm, in Eq. (13), which is also the reason behind normalizing the disturbance inputs w and the performance outputs z.

$$\|F_l(\boldsymbol{G},\boldsymbol{K})\|_\infty = \max_{w\neq 0} \frac{\|z\|_2}{\|w\|_2} \tag{13}$$

In the present contribution, the disturbance inputs are forces acting on the system, namely the unbalance force and the force due to the weight of the rotor; the performance outputs are the control current and vibration levels.

7 Numerical Results and Discussion

The results will compare the two types of controllers pursued, standing for: (i) the controller searching simply for vibration suppression, and (ii) the controller allowing for crack detection, by keeping the 2X and/or 3X vibration harmonics in the spectrum. Both LQR and H_∞ controllers will be compared, concerning these two different aspects. The system is expected to be capable of shifting from one controller to another, as necessary, for performing SHM of the rotating machine. The appropriate shifting time depends on the machine characteristics and will not be considered here.

The simulations were performed by considering the non-dimensional equations. Some variables are set to present always the same value, which are $\xi = 0.02$, $k_\eta = 1$, and $\beta = 0$. Additionally, random noise was added to all the dynamic responses of the rotor, to simulate an experimental environment, as found in a real plant. Equation (14) indicates how noise was added to the system responses.

$$\boldsymbol{q}_{noise} = \boldsymbol{q} + P_{noise}\boldsymbol{R}_{noise}\left\{E[\boldsymbol{q} - E(\boldsymbol{q})]^2\right\}^{1/2} \tag{14}$$

where $\boldsymbol{q}_{noise}$ is the noisy response, P_{noise} is the parameter that defines the amount of noise to be added ($P_{noise} = 5\%$), and $\boldsymbol{R}_{noise}$ is the random noise, with zero mean and unitary standard deviation. $E[\cdot]$ indicates the expected value of $[\cdot]$.

7.1 Sub-Critical Speed: $\boldsymbol{\Omega} = 0.3$

At this sub-critical speed, a healthy and a cracked rotor produce vibrations due to the unbalance force, which are presented in Fig. 4. For this result, an incipient crack with a stiffness ratio of $k_\xi/k_\eta = 0.9$ was considered. All sub-critical speed results assume a non-dimensional unbalance value of $U = 8$ (respecting the weight dominance condition).

Note that the healthy rotor produces perfect sinusoidal waves and possesses only the 1X vibration component over the FFT response, which is related to its unbalance

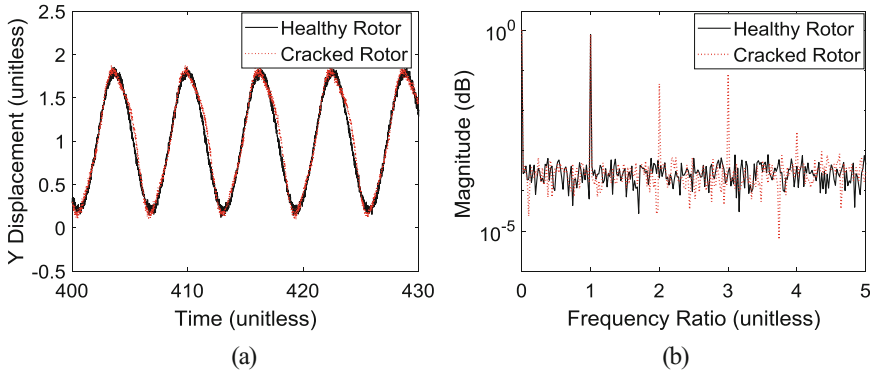

Fig. 4. Vibration signals - healthy and cracked rotor: (a) Time domain; (b) Frequency domain.

force. On the other hand, the FFT response associated with the cracked shaft presents the 2X, 3X, and 4X vibration components in addition to a small increase in the 1X harmonic as compared with the response of the healthy shaft.

Figure 5 presents the first comparison between *LQR* and H_∞ controllers. With both techniques, it is possible to obtain around 97% of vibration suppression for the vibration-based control configuration. As expected, all the super-harmonics were suppressed (in the presence of noise) by both the controllers, thus avoiding the application of crack detection strategies.

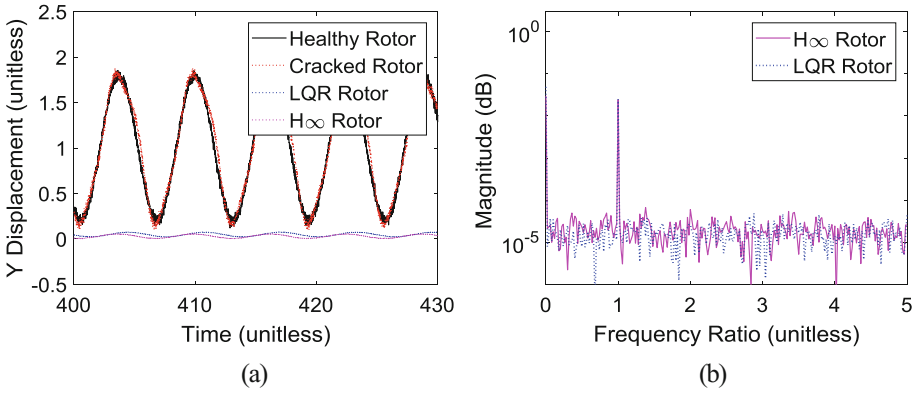

Fig. 5. Control dedicated to vibration suppression: (a) Time domain; (b) Frequency domain ($Q * inv(R) = 25 * eye(2)$; $x_{max} = 0.5$; $i_{max} = 10$).

For enabling performance comparison between *LQR* and H_∞ synthesis regarding crack detection, one should determine a minimum amplitude at which crack detection techniques can be applied. In Bently and Muszynska [22], the minimum value of the super-harmonic 2X is defined as the one that permits visual detection. Figure 6(b) presents what is considered in this paper as the minimum value of the 2X component

capable of clearly detecting the existence of a crack in the frequency spectrum. For illustration purposes, the authors have chosen a non-dimensional magnitude of $2.5x10^{-3}$ above the noise level. Obviously, this value should be redefined according to each machine.

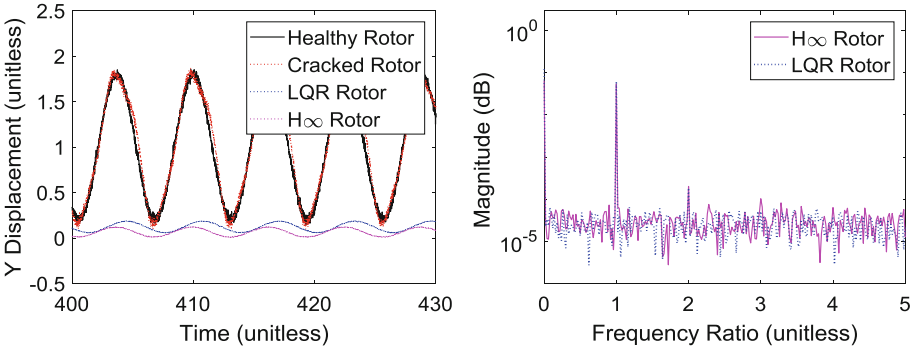

Fig. 6. (a)Time and (b) frequency responses for the case without control and for the controlled case by using *LQR* and H_∞ synthesis ($Q * inv(R) = 4 * eye(2)$; $x_{max} = 1.1$; $i_{max} = 10$).

It is also important to note that there are other malfunctions that may impose variations over the 1X, 2X and 3X magnitudes, such as unbalance, misalignment, thermal bow, rubbing, etc., as discussed in [22, 23]. Thus, the existing super-harmonics levels should be taken into account for defining the new amplitudes for crack detection purposes [22].

Finally, Fig. 6 shows the case where the maximum of vibration suppression was applied, respecting the threshold defined for detecting an incipient crack, $k_\xi/k_\eta = 0.9$.

Both the controllers presented close results, i.e., the H_∞ controller was able to reduce 94% of the shaft vibration amplitudes, while the *LQR* controller was able to reduce 92% of the vibration amplitudes. This is considered an interesting result, since it was demonstrated that shifting the controllers does not compromise the safe functioning of the rotor system (optimum control: 94%; control allowing for crack detection: 92%).

Although it can be sustained that the *LQR* control represents a simpler option for implementation and tuning, some difficulties may appear in real-life applications. On the other hand, H_∞ synthesis is more complex for both tuning and implementing, but it may be expanded to account for system uncertainties in the form of a μ-synthesis controller, resulting potentially on a more effective and applicable control strategy.

Figure 7 stands for the behavior of the 1X and 2X components, as the crack grows from a stiffness ratio of $k_\xi/k_\eta = 0.95$ to $k_\xi/k_\eta = 0.75$, for both the controlled and uncontrolled conditions. It was observed that the rotor without control presents an exponential growth according to the crack depth, while for both the controllers used this growth is much slower and tends to be more linear.

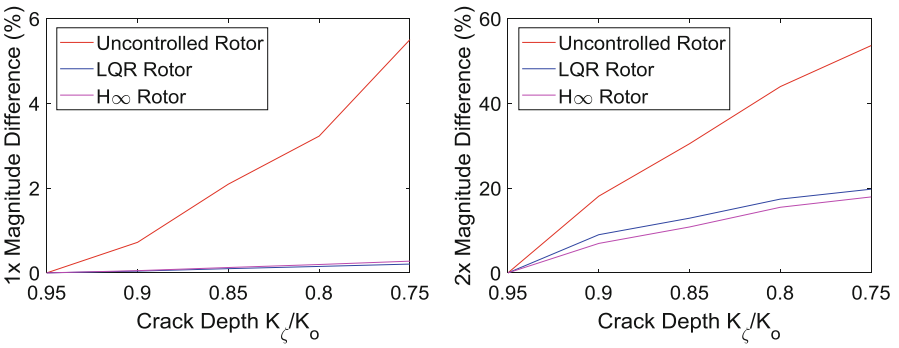

(a) (b)

Fig. 7. Magnitude percentage growth for the components (a) 1X; (b) 2X, as a function of the depth of the crack, for sub-critical speeds ($Q * inv(R) = 4 * eye(2)$; $x_{max} = 1.1$; $i_{max} = 10$)).

7.2 Super-Critical Speed: $\Omega = 1.3$

For the rotor operating at super-critical speeds, it is necessary to guarantee smaller values of unbalance, so that the weight dominance condition is respected (see Fig. 8 (a)). As mentioned earlier, for the super-critical speed of $\Omega = 1.3$, the unbalance parameter considered was $U = 0.4$. All the other parameters were kept with the same values as for sub-critical speed. Thus, the rotor vibration without control are depicted in Fig. 8.

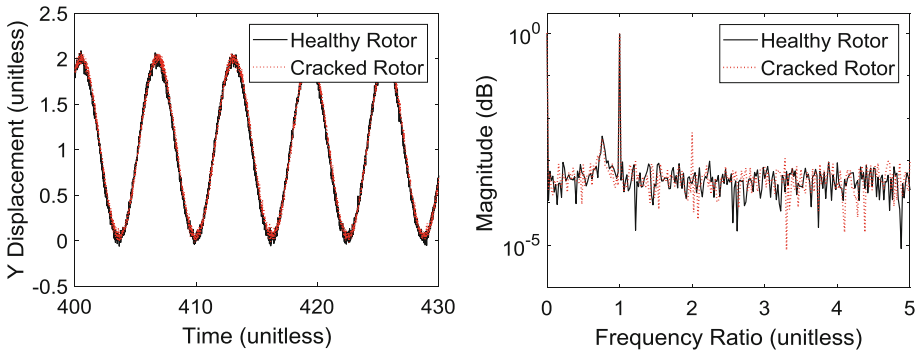

(a) (b)

Fig. 8. Vibration signals: healthy and cracked rotor: (a) Time domain; (b) Frequency domain.

For super-critical speeds, in general, crack detection appears to be much harder. Note that the 2X and 3X components, Fig. 10(b), possess much less energy, being this last covered by the noise. Even for this case, both techniques were able to reduce 98% of the rotor vibration amplitudes (control dedicated to vibration-based control only) (Fig. 9).

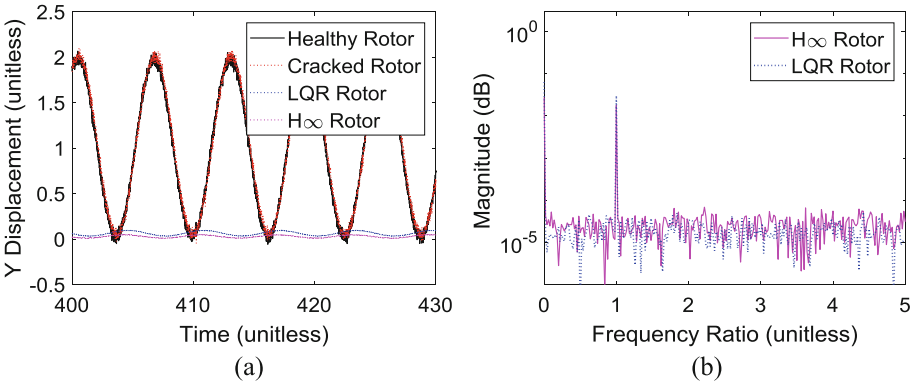

Fig. 9. Control dedicated to vibration suppression: (a) Time and (b) Frequency domain ($Q * inv(R) = 15 * eye(2)$; $x_{max} = 0.5$; $i_{max} = 10$).

In the sequence, Fig. 10 presents the efficiency of the H_∞ controller, which is expected to allow for crack detection, by keeping the minimum amount of energy on the 2X harmonic.

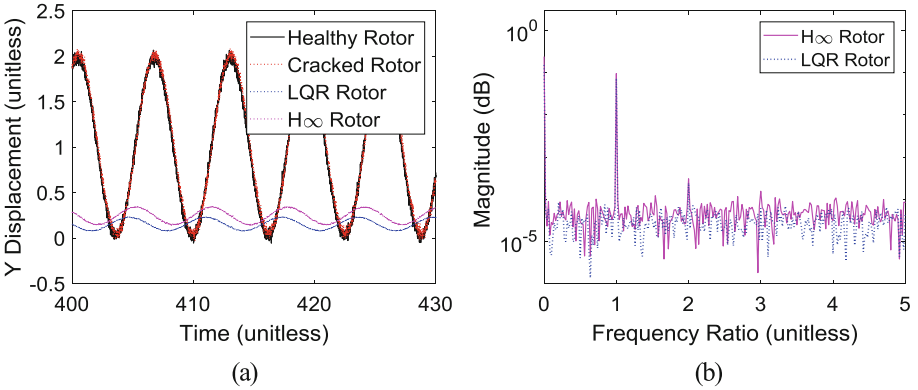

Fig. 10. (a) Time and (b) frequency responses for the rotor controlled by *LQR* and H_∞ controllers ($Q * inv(R) = 2.5 * eye(2)$; $x_{max} = 2.5$; $i_{max} = 5$).

Again, at this super-critical speed, H_∞ and *LQR* techniques presented similar results, being capable of reducing 92% and 90% of the shaft vibration amplitudes, respectively. The same threshold was kept, since the indicator in this paper was chosen to be simply visual. Again, an interesting result was found for this super-critical rotation speed, resulting a smooth transition between the controllers.

The study of the percentage of growth for the 1X and 2X components, according to the increase of crack depth is shown in Fig. 11 for super-critical speed.

Note that for the uncontrolled case, the 1X component grows more critically than it was found for the sub-critical condition, tending now to present a more linear behavior,

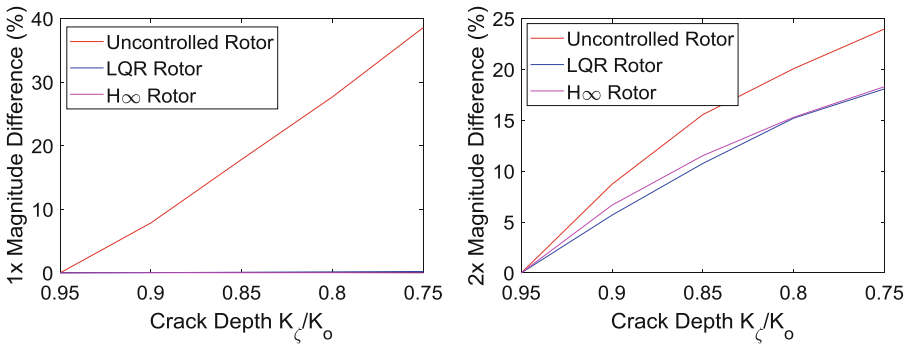

Fig. 11. Magnitude percentage growth for the components: (a) 1X; (b) 2X, as a function of the crack depth, for super-critical speeds ($Q * inv(R) = 2.5 * eye(2)$; $x_{max} = 2.5$; $i_{max} = 5$).

reaching 38% growth for $k_\xi/k_\eta = 0.75$, while for both controllers this magnitude only increased about 0.3%. The magnitude of the 2X component presented a similar behavior, but smaller differences were observed for the uncontrolled case. In general, one can conclude that the controlled rotor presents much smaller vibration growth, which can offer a larger period of time for the crack to be detected before a potential failure occurs.

8 Conclusions

In this research effort, the effects of *LQR* and H_∞ control techniques were compared considering two different scenarios that were taken into account for a rotating machine that was represented by a Jeffcott rotor model: control dedicated to vibration suppression, and a control allowing for crack detection. It can be concluded that the use of any of these controllers, aiming simply at vibration control, can completely suppress the 2X and 3X harmonic components, for both sub-critical and super-critical speeds (mean of attenuating around 97% of the rotor vibration). On the other hand, the results also showed that it is possible to maintain the 2X and 3X harmonics and still observe a satisfactory level of vibration suppression for both the controllers (sub-critical and super-critical speeds - attenuation around 92% of the rotor vibration). Since the observed attenuation levels for both scenarios were close, the system can safely switch, as necessary, from one configuration to the other. The effects of both *LQR* and H_∞ controllers over the analyzed rotor model were very similar, which means that the use of a more sophisticated control strategy will not necessarily present better results concerning the two objectives of this contribution, namely vibration suppression and health monitoring. Therefore, the control engineer can choose a preferable strategy according to the operation convenience, remembering that the *LQR* stands for an optimal controller, whereas the H_∞ control can deal with uncertainties, resulting a robust controller. Finally, the results showed that when a cracked rotor operates with any of the controllers, its vibration amplitudes grow much slower than for the

uncontrolled case, giving the system an extra for crack detection. An experimental verification of the methodology conveyed is scheduled for the near future.

Acknowledgements. The authors are thankful to the financial support provided to the present research effort by CNPq (574001/2008-5) and FAPEMIG (TEC-APQ-3076-09 / TEC-APQ-02284-15), through the INCT-EIE.

References

1. Kasarda MEF (2000) An overview of active magnetic bearing technology and applications. Shock Vib Dig 32(2):91–99
2. Schweitzer G (2009) Applications and research topics for active magnetic bearings. In: IUTAM-symposiumon emerging trends in rotor dynamics, Delhi
3. Kulesza Z, Sawicki JT (2012) Controlled deflection approach for rotor crack detection. J Eng Gas Turbines Power 134(9):92–102
4. Pesch AH, Hanawalt SP, Sawicki JT (2014) A case study in control methods for active magnetic bearings. In: Dynamic systems and control conference, San Antonio
5. Imam I, Azzaro SH, Bankert RJ, Scheibel J (1989) Development of an on-line rotor crack detection and monitoring system. J Vib Acoust Stress Reliab Des 111:241–250
6. Sawicki JT, Friswell MI, Kulesza Z, Wroblewski A, Lekki JD (2011) Detecting cracked rotors using auxiliary harmonic excitation. J Sound Vib 330:1365–1381
7. Litak G, Sawicki JT (2009) Crack identification by multifractal analysis of a dynamic rotor response. ZAMM Z Angew Math Mech 89(7):587–592
8. Litak G, Sawicki JT, Kasperek R (2009) Cracked rotor detection by recurrence plots. Nondestruct Test Eval 24(4):347–351
9. Sawicki JT, Sen AK, Litak G (2009) Multiresolution wavelet analysis of the dynamics of a cracked rotor. Int J Rotat Mach
10. Kulesza Z, Sawicki JT (2010) Auxiliary state variables for rotor crack detection. J Vib Control 17(6):857–872
11. Kulesza Z, Sawicki JT, Gyekenyesi AL (2012) Robust fault detection filter using linear matrix inequalities' approach for shaft crack diagnosis. J Vib Control 19(9):1421–1440
12. Zhu C, Robb DA, Ewins DJ (2003) The dynamics of a cracked rotor with an active magnetic bearing. J Sound Vib 265:469–487
13. Gasch R (1976) Dynamic behaviour of a simple rotor with a cross-sectional crack. In: IMechE conference on vibrations in rotating machinery, Cambridge C178(76), pp123–128
14. Gasch R (1993) A survey of the dynamic behavior of a simple rotating shaft with a transverse crack. J Sound Vib 160:313–332
15. Mayes IW, Davis WGR (1976) The vibrational behaviour of a rotating shaft system containing a transverse crack. In: IMechE conference on vibrations in rotating machinery, Cambridge, C168(76), pp 53–64
16. Mayes IW, Davies WGR (1984) Analysis of the response of a multirotor-bearing system containing a transverse crack. J Vib Acoust Stress Reliab Des 106:139–145
17. Friswell MI, Penny JET, Garvey SD, Lees AW (2010) Dynamics of rotating machines. Cambridge University Press, Cambridge
18. Burbano CR, Steffen Jr. V (2007) Diagnosis of cracked shafts by monitoring the transient motion response. In: International symposium on dynamic problems, SP, pp 1–10
19. Singhal S (2014) Motors not turbines drive heavy equipment. In: Machine design

20. Pandey SK, Laxmi V (2015) Optimal control of twin rotor MIMO system using LQR technique. In: International conference on CIDM, v 1, pp 11–21
21. Maslen EH, Sawicki JT (2007) Mu-Synthesis for magnetic bearings: why use such a complicated tool? In: IMECE 2007, Seattle
22. Glover K, Doyle JC (1988) State-space formulae for all stabilizing controller that satisfy an H∞ norm bound and relations to risk sensitivity. Syst Control Lett 11:167–172
23. Bently DE, Muszynska A (1986) Detection of rotor cracks. In: Fifteenth turbomachinery symposium, Texas, pp 129–139
24. Bachschmid N, Pennacchi P, Tanzi E (2000) Identification of transverse crack position and depth in rotor systems. Meccanica 35(6):563–582